JCBI
Journal of Computing & Biomedical Informatics Volume 03 Issue 01
ISSN: 2710 - 1606 2022

Research Article

Deep Learning Techniques for Diagnosis of Lungs Cancer

Rabia Javed[1*], Azka Sarfraz Khan[2] and Ali Haider Khan[2]

[1]Department of Computer Science, TIMES Institute, Multan, 60000, Pakistan
[2]School of System & Technology, Department of Computer Science, University of Management and Technology Lahore, Lahore, 54770, Pakistan
[*]Corresponding Author: Rabia Javed. Email: 786rabiajaved@gmail.com

Received: December 28, 2021 **Accepted:** February 19, 2022 **Published:** March 15, 2022

Abstract: Low_dose computed tomography (LDCT) scans are widely used to diagnose early cancers. Clinical studies show that low CT scans reduce lung cancer by 20% compared to standard radiography. However, conventional low-intensity CT scans are prone to overuse, high cost, and increased radiation exposure. This paper seeks to address these challenges by developing machine learning and in-depth case studies for automated cancer screening and assessing disease progression. The new split-method approach was first developed using two-sided select methods and machine learning methods. This method is designed to include ring nodes mounted on the ring bar but significantly reduce partition errors. Second, a neural network is being developed to classify clean nodes according to non-nodes. The simulation model integrates VGG, residual, and multi-network module design to enhance the dynamics of external collection components and various reception constraints. Third, the Hierarchical Semantic Convolutional Neural Network (HSCNN) is defined to form negative nodule rings. The semantic components, predicted to be equal to the deficit per node, facilitate the definition of this type and the improvement of visual acuity. Finally, the Bayesian design as well as the full-time Markov version have been improved. The decision-making process selects the exchange of information about the individual cancer, providing the basis for a special research study. Numerous experiments and results have shown the effectiveness of these experimental methods in improving and enhancing the efficiency of low-frequency CT programs.

Keywords: Lungs cancer; Deep learning; Typeset, Low dose computed tomography, Split Method.

1. Introduction

Lung cancer is the foremost basis of cancer demise in both women and men. The five-year survival rate is only 17% for lung cancer, but if detected early, the survival rate increases to 54%. Low-Dose Computed Tomography (LDCT) is the actual imaging method currently used to detect and diagnose lung cancer, with 20% mortality for people undergoing. National Lung Screening Trial (NLST) compared to flat chest radiography. Associated with conventional chest radiography, CT provides large, accurate, comprehensive data sets that can undertake small and/or low-contrast nodules. Nonetheless, there are several problems with the use of LDCT in this context, which hinders accurate detection and effective selection. First, screening programs provide large data sets that require time and effort to be carefully examined by radiologists. Second, less experienced radiologists, especially in rare cases, have very different detection rates because interpretation is based on previous experience. In fact, it is often difficult to distinguish malignant nodules precisely from benign lesions, resulting in a high degree of false-positive results [1] As found during NLST, positive prognostic values for LDCT (i.e., the ratio of positive screens with subsequently confirmed lung cancer diagnosis) were only 3.8, 2.4, and 5.2%, respectively, in indications 1, 2, and 3. Finally, concerns about radiation exposure, over-diagnosis, and overtreatment underscore the need for

more personalized screening to determine who should be examined and how often. This dissertation focuses on improving lung cancer screening and diagnosis with new types of machines and in-depth training to overcome these challenges, including 1) automatic lung replacement; 2) computer-assisted diagnosis of nodules and diagnosis of lung cancer in CT images, and 3) periodic personal evaluation of the selection period. Experimental studies show that three small diagnostic CT programs have three problems: 1) high prognosis, 2) high cost, and 3) increase electrical conductivity. The NLST study reported a poor negative ratio of 96.4% for overall positive test results. According to NLST results, the cost is $ 52,000 and $ 81,000 per year of life and one year of quality of life (QALY) per capita. In all, 10,000 subjects surveyed were selected to die in about 1-3 cases as a result of radiation exposure[1]. The development of computer-assisted diagnostics / diagnostic procedures (CAD/CADe) and the implementation of self-assessment procedures are considered to be the best keys to solving these problems. The CAD/CADe methods used a combination of machine learning (e.g., vector support equipment, decision rods) and numerical techniques to diagnose and diagnose cancer [2]. It has been a field of research in the field of health imaging for the past two years. CAD/CADe systems have been established to assist radiologists in the reading process, which may increase the prognostic value in diagnosing tuberculosis for small nodules compared to human readings and reducing bad numbers not good by radiologists[3]. CAD / CADe projects are shown to perform our analysis.

The diagnostic workflow of CAD / CADe normally consists of four main components, as shown in Figure 2: 1) Inhibitory zone 2) Nodule candidate generation; 3) Nodule insertion; 4) Chronic obstructive pulmonary disease. The first step is to Region Of Interest (ROI) for most CAD / CADe systems for later analysis (i.e., lightweight). The most commonly seen lung nodules in the anatomical unit are the juxtapleural nodules (as shown in Figure 1)[4]. Although many procedures have been performed to regulate the distribution of the lungs, only a few still retain pleural nodules. And lack of evaluation. The goal of the second stage is to use a common threshold and morphological process to isolate a large number of suspected nodule candidates from these high-level ROIs. In the third stage, a hand-held model is used to separate lymph nodes and non-modular lymph nodes (e.g., parts of arteries, blood vessels, and non-cancerous lesions)[5]. And the wailing alarm. Finally, the candidate selects lung nodule as malignant or non-malignant. Medical information, features, functions, and radiation features are used in these modeling

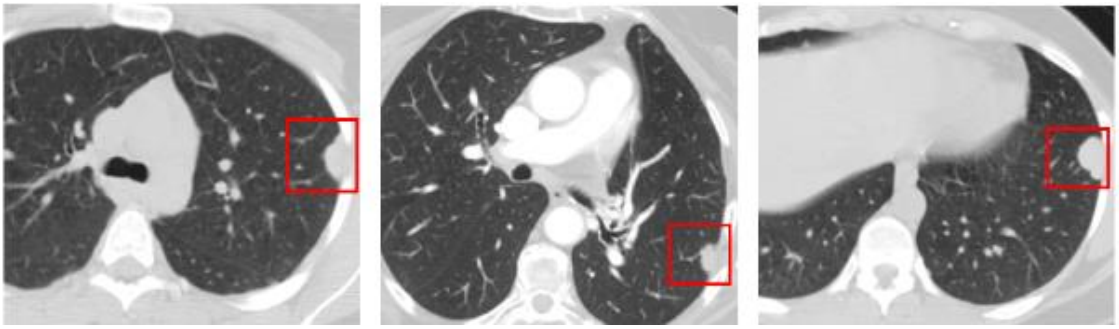

Figure 1 Visual of juxtapleural nodules. [1]

techniques[6]. It should be noted that although many types of diagnostic techniques are involved in the process of nodule recurrence/diagnosis, most of them are inconsistent with the performance of external data. Increasing research analysis opens the possibility of examining the history of lung disease and creates opportunities for individual observation to conduct systematic and effective clinical research[7]. As shown in Figure 2(b), the incidence of breast cancer is usually measured gradually in three states: stateless (Stage 1), asymptomatically advanced state-based (Stage 2), and position (Stage 3). Mean Sojourn Time (MST) measures the severity of illness from hospital to hospital. Numerous statistics and physical methods have been developed to inform MST, such as the Markov brand and alternative methods. Despite the best efforts, it is difficult to compare MSTs of different groups using conventional methods due to inaccurate identification and complexity. This study considers three areas that address some of the previously mentioned challenges: 1) bright divisions; 2) node and identification group; and 3) examples of cancer progression. The next three sections are described in more detail by what motivates each activity[8].

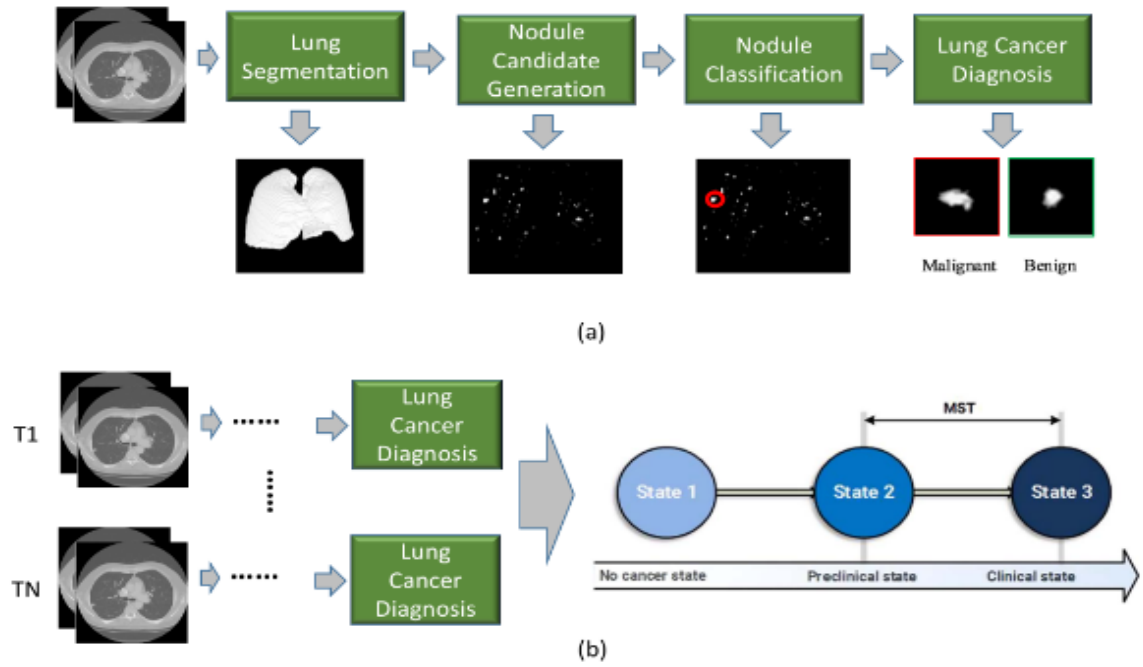

Figure 2 Computer-assisted diagnosis of lung cancer and prognosis

Lung separation is a critical precursor to a lung node CAD system, where the lung area is acquired and becomes a region of interest for detection and/or screening tasks. This step defines the sensitivity of high visibility connection for the whole system since the nodules in a "non-agricultural" region are not detectable and detectable[9]. Juxtapleural nodules are a class 4 of the most lost lung nodules. Although many studies have planned the automatic distribution of thick images of CT breasts, there is little clear treatment for the presence of juxtapleural nodules. Among the existing works focusing on juxtapleural nodules, most rely on one (or more) predefined parameters, making the algorithm sensitive to differences in the shape and size of the pulmonary nodule[10]. For example, a "rolling ball" technique is used to reconstitute just-pleural nodules for lung separation, consisting of a near morphological operator with a structurally shaped element. The effectiveness of morphological operations depends on the predetermined "ball." Because the size and shape of the vertebrae of the spine vary, it is difficult to choose the right size that will normally work in all situations[11]. For example, small parts of the structure will not capture large nodules; on the contrary, large sections of the structure will cause extreme segregation and weakness of local spaces. In addition, reviews of these works often do not contain or use small experimental tools (as in most cases), which cannot represent the full range of such spice characteristics (such as changes in size and shape). Therefore, there is a great need for a new system of lung separation without parliaments to solve problems related to application loopholes[12].

This paper presents innovative techniques of thinking and in-depth instruction that provide the gap between screening and prompt exposure of early cancer. Develop a method of simple separation without boundaries. This type of double chain fixation prevents the edges of the yeast cells from preventing the removal of light nodules that have been brought to the boundary while reducing to the left. Develop strong support to transfer nodule lung information and translation ideas for the treatment of tuberculosis with neural convulsions. A known limitation of the current workload is that most of the proximity offers are given to minimize the work without any technical knowledge. A hybrid ensemble of a consular neural network has previously been developed to detect pulmonary nodules associated with VGG, residuals, and those taken in relative to each other, transmitting effects such as inconsistencies found in independent documents without proper correction[13]. The Hierarchical Semantic Convolutional Neural Network has been described as a guideline for the diagnosis of cervical cancer with semantic radiological interpretive

applications[14]. This HSCNN model reflects the semantic features proposed by a given radiologist while predicting nodal aggregation, all of which have classification. Predictions from this semantic neural network can be used to understand how the model works, in addition to serving as a semantic feature generator for unlabeled imaging datasets.

2. Literature Review

Lung cancer is the leading cause of cancer-related deaths worldwide. The American Cancer Society estimates that lung cancer was responsible for 27% of all cancer-related deaths in 2015; the average 5-year survival rate was only 17%[15]. One of the key facts regarding the low survival rate is that only 15% of lung cancers are diagnosed at an early stage without obvious cancer symptoms. On the contrary, if lung cancer is caught early, the survival rate will increase to 54%. The early detection of lung cancer is a driving factor, and research is currently underway to improve the recognition of newborn diseases.

2.1 Calculated tomography for screening for Lung Cancer

Computed tomography (CT) is currently the most widely used screening method for detecting early-stage lung cancer. In 2011, the National Lung Screening Trial (NLST) measure showed a 20% decrease in mortality in lung cancer patients screened (LDCT)with low-dose CT compared to simple chest photographs[16] Based on this evidence, the USPSTF (USPSTF) then issued a Grade B recommendation to conduct an annual screening for Low-Dose CT (LDCT) in adults aged 55 to 80 years[17]. He smoked a pack 30 years ago (the number of cigarettes smoked per day multiplied by the number of years a person smoked) and currently smokes or has stopped smoking in the last 15 years. This policy has stimulated the development and implementation of new lung cancer screening programs using LDCT.

2.2 Computer-aided Diagnosis (CAD)

Computer-Aided Design (CAD) is an important part of investigating healthy images. The basic concept of CAD is to use the computation of an algorithm (computer program) as a 'second idea' to help radiologists interpret the process of detecting patients. CAD has two broad goals. 1) Improving the consistent reading of radiologists; and 2) shorten the drawing time. The standard design for CAD is to identify (reference) disease sites (e.g., lions) with one or more medical images/pictures. And/or establish a specific reference point for the presence of the disease. Both programs are similar to CAD for diagnostics and CAD for general information. Other techniques associated with these CAD drawings include: 1) drawings for drawing and identifying inappropriate objects (separation); 2) creating an image representing an unqualified candidate; 3) Classify candidates by image type (positive or negative) that distinguishes normal and adventitious muscles

2.3 Deep Learning Approaches

Traditional methods of machine learning have limited ability to process local data in the original format (the size of the original image), so they rely on service engineering and information fields to identify and assign significant values to the original data from the learning agency. Conversely, the representation of the study in a range of methods that can reflect the best images and services to accomplish tasks related to planning / estimating / finding. Intensive learning is a learning process that represents an attempt to convert raw data into integrated demonstrations by combining different processing modules[18]. The point of in-depth study is that these components of the services are studied in raw data using a more common learning process than the model developed by engineers. Advanced learning techniques have been used in a variety of activities to discover and edit and significantly improve the level of basic skills, such as speaking and understanding of symbolism, object acceptance, and the use of the original language[19]. These achievements also demonstrate that the ability to fully learn to represent and integrate complexities into high-quality data related to traditional engineering. Extensive research can lead to greater success in the future because it requires less manual labor.

Various deep learning approaches are offered, including deep-enhanced trust, Boltzmann's advanced machines, repetitive neural networks, compressed auto encoders, and a convoluted neural network[20].

The next method, which is an observational method of reading, has attracted the most attention in this research paper and has been introduced in the following sections.

2.4 Multi-state Syndrome Evolution

An improved perceptive of the diminuendos and progression of lung cancer, for instance, the time anticipated to extend a specific disease stage, might guide to additional apposite avoidance, treatment, and management; over and above primary exposure. Periodic imaging is one of the utmost corporate techniques to detect lung cancer in the early stages. Longitudinal data collected as a result of screening provide the opportunity to discover improved methods to characterize the natural progression of the disease and generate predictions for individual screening or diagnostic policies. Traditionally, a "one size fits all" approach has been used to display programs; however, patients at lower risk for cancer should have longer screening periods or none at all. The MST measures how rapidly a disease progresses from a preclinical (image-observable but not observable) to a clinical (with) observable symptoms), and has been widely used to model disease progression and does not include the size of the screening population, to calculate the ideal interval between performances and estimate the extent of over diagnosis.

Several strategies have been proposed, for example, for multinational diseases, especially for MST. Aalen et al. Demonstration of HIV/AIDS using the Markov model; Chen et al. determine the three states of the breast cancer model. Many state-of-the-art Markov cities can adjust the resolution of continuous data in the absence of scattering interference. In some words, they have been used as examples of atherosclerosis, high blood pressure, stroke, and diabetes[21]. Duffy et al. use a three-position Markov for regular long-term breast cancer tests to calculate the sensitivity of MST and diagnostic systems. This method calculates the best way to calculate the state conversion time and then calculates the correction using the conversion time.

2.5 Coherent image of Raman scattering in human lung tissue

Figure 3 shows CARS images at the cellular level (upper plate) and equivalent H&E discoloration outcomes(lower plate) from conventional adenocarcinoma tissue, squamous cell carcinoma, and small cell lung cancer[22]. The normal lung consists predominantly of a well-organized fibrous elastin and collagen structure (shown as a glossy structure in Figure 3 (a)) that exertion together to maintain and complete lung tissue. Build a sexual support network. Elastin makes up about 50% of the binding mass of the lungs and acts as a flexible protein that allows the lung tissue to regain its unusual shape after distending. Collagen fibers are well-positioned proteins that help conserve the malleable potency of the lungs for the period of the respiratory practice. In divergence, cancerous lung bones no longer retain rich fibrous structures, as cancer progression is often accompanying with destruction and rupture of the imaginative matrix complex in the anterior invasive part of the eardrum. Thus, cells A 3 (b) –3 (d) show a denser cell and a much less fibrous structure than in normal samples. Because the nuclei (yellow arrow) have less CH2 binding to the cell membrane and cytoplasm, they appear as dark spots in CARS images.

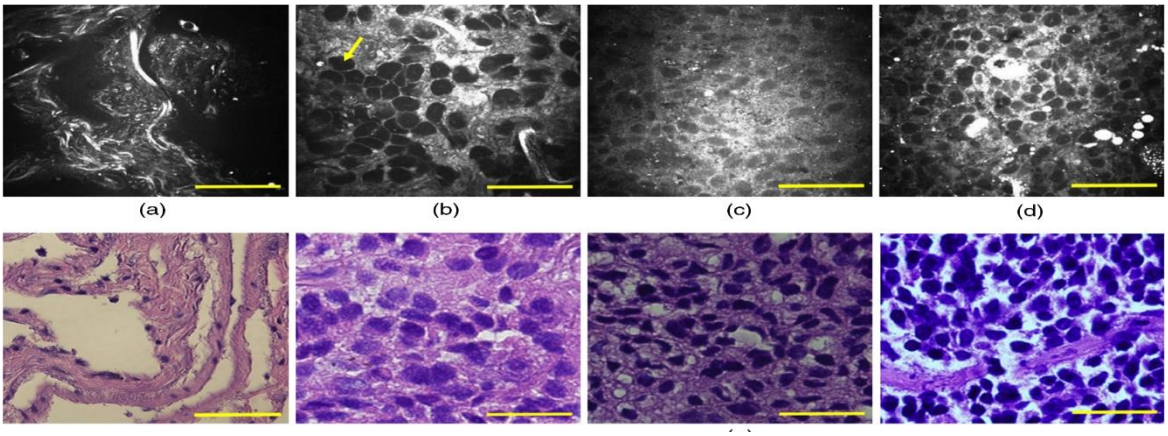

Figure 3 :[1] The CARS image represents (upper arm) and the corresponding H&E image (lower arm) of the human liver: (a) and (e) normal lung, (b) and (f) adenocarcinoma, (c) and (g)) squamous cell carcinoma, and (d) and (h) small carcinoma. Rotation bar: 50 μm.

The material can usually be identified using three types of neoplastic. Adenocarcinoma mostly has cancer cells in a large surrounding area and covers the vesicle nuclei, and various cytoplasm form the glandular shape. Only a few broken elastin and collagen are found in the tissue. An example of squamous cell carcinoma is a polymorphic disease cell line with a large cytoplasm and intracellular layer. Small cell carcinoma can be observed by round / elliptical cells with high nuclear-cytoplasmic release. All CARS pictures show a good pathological correlation with H&E stained parts in the same tissue sample[23]. There were fewer observed differences between CARS imaging and histology, while color inconsistencies in H&E imaging were associated with tissue fixation, processing, staining, and item cutting. Due to the small FOV imaging of CARS and the small working distance from the target, it is difficult to find the exact picture point, which can also cause inequalities between H&E and CARS imaging.

2.6 Automated classification and diagnosis of lung tension differentiation

First, a 9x integrated validation method is used to test the effectiveness of motion learning on CARS images. The complete set of training and validation data is divided into nine folders (folders are divided into groups of unconnected patients). Hold one fold each time as a test set and train the model with the remaining eight folds of data so that each of the nine folds works as a test set. The overall accuracy achieved with the retraining model was 89.2% ± 2.1% (± SD minimum). The learning transition from the course and the validity of one component set up by Tensor Board are shown in Figure.4. A stochastic gradient down-link optimization algorithm is used to reduce costs. Sixty-four pictures were randomly selected from each training session to be able to compare each type of model. The task of training is to prove the value in Figure 4. They both came down and hit a little later 40,000 steps.

Figure 4 [1] Study Curve Learning is a one-time validity test conducted by Tensorboard. Short-term noise occurs because the potential gradient for the algorithm is reduced. The curves are smoother to ensure better visibility.

The rehearsed model was then tested on a container test set that he had never seen before. The model has an accuracy of 91.4% forecast, which indicates that it is strong for data. Figure 4 shows the standard problem matrix for maintaining the test set. Each row represents the true part of the earth, and each column represents the type prophesied. Here see that 100% of the real standard cases are correctly classified. About 95% of lung cancer cases have been successfully diagnosed with small-cell lung cancer, and 4% of them have been diagnosed with lung cancer[24]. It also like to remind you that the two NCL substitutes are

sometimes incompatible with each other, especially in areas that are not well defined. These are characteristic of adenocarcinoma and cancers and are consistent with clinical trials.

As a result of the unequal distribution of the category labels in the data, the Receiver operating characteristic curve (ROC) is designed under three conditions see Figure. 5. Separate the lung cancer image from the normal lung image. (2) Non-small cell lung cancer pictures are separate from non-small cell lung cancer pictures. (3) Subtypes of single lung imaging for non-small cell lung cancer, i.e., adenocarcinoma and squamous cell lung cancer. The ROC curve shows the false positive level (1-specificity) on the X-axis and the true positive level (sensitivity) on the Y-axis. In particular, the real positives in each case are: (1) the correct estimated number of lung cancers; (2) the correct estimated number of small cell images; and (3) the estimated number of correct images of adenocarcinoma lungs. If the CARS image is fed by a model, the final classification layer provides a normal distribution of the four classes (normal small cells, adenocarcinoma, and squamous cell carcinoma). For each condition, the ROK curve is determined by determining the true positive rate in different boundaries with the false polo positive rate[25]. The curvature field (AUC score) was also calculated for each condition, and about 1 AUC score was a very good diagnostic test. From a medical point of view, reducing false negatives (known as type II errors) is more important in the diagnosis of cancer, as the absence of cancer makes the patient unable to receive treatment.

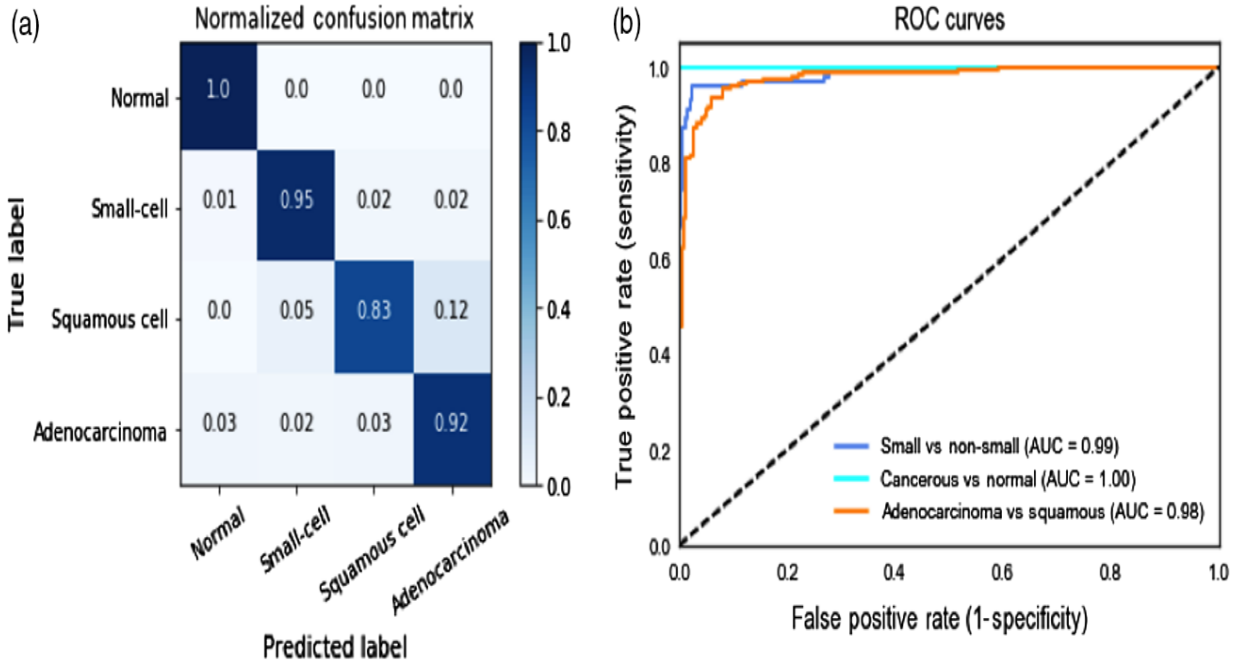

Figure 5 CNN practice is deeply involved in test performance. (a) Normal matrix blockage. Each row compares different examples, and the real-time and values in each column represent a somewhat predicted percentage of the image. (b) ROC procedure for three reason

In order to well comprehend the core characteristics of the redesigned model under study, the last layer is being visualized using the adjacent random insert with t distribution (t-SNE) in Figure 6. Each point in Figure 6 shows CARS Images from the test set. The color reflects your reality. The original 2048-dimensional output of the last layer of the model has been reduced and displayed in the 2-D plane. t-SNE primarily converts the similarity between the data points into joint probability and attempts to reduce the Kullback-Leibler difference between the joint probability of low-dimensional and high-dimensional data. Points belonging to the same class should be closely grouped. As can be seen in Figure 5, almost all normal cases are clearly grouped according to the result of the confusion matrix. Some poorly classified small cells occur in cases of squamous cell carcinoma[26]. Likewise, there is a correspondence amongst adenocarcinoma and squamous cell carcinoma. This is because these two subtypes of lung cancer have significant pathological similarities.

Neural networks have been called "black boxes" for a long time because of the large number of non-linear interacting parts, and it is challenging to comprehend accurately how an especially competent neural network works. 66 represents the first convolutional layer. In Figure 6, you can see some traditional image descriptors designed for object recognition, such as identifying the edges of cell nuclei and identifying circular lipid points[27]. Looking at the inner convolution layer can give us a good intuition about the convolution operation in the CNN depth model.

Figure 6 Visualization of the first conceivable layer of the Google3 Net Inception V3 standard for general CARS images and with a small lung cancer cell. The first convex layer has 32 cores measuring 149 × 149 pixels.

Figure 6 t_SNE view of the final cover on CNN (image 758-CARS) at a depth of the test set. Colored dotted clouds correspond to four diverse individual lung materials collected by the set of rules. Red dots are regular manifestations of the lungs, and blue dots a

3 Methodology

In this session, a robust model of automatic classification of lungs and nodes is presented using a hybrid ensemble of multiple CNN. This model was first built on a large data set known to the public and then independently validated externally without re-reading the model in the data set. Second, it characterizes the controversial network of deep tissue semantic cross-linking for the prediction of lung cancer with two levels of outcome[28]. 1) Semantic features of a low-level radiologist; and 2) high malignancy prognosis scores. Low-level semantic results measure the diagnostic features used by radiologists and describe how the model images are interpreted by specialists. In the remainder of this article, a modified CNN ensemble is developed for the detection of lung nodes and an HSCNN model for the diagnosis of lung cancer

3.2 A hybrid ensemble CNN model for lung nodule classification

In this study, only images with a disc thickness of less than 3 mm were recorded, resulting in 897 LIDC CT scans. Four radiologists marked the contours and functions of the nodes in the LIDC for each CT scan but did not reach a mandatory agreement on the presence of the nodes. Therefore, depending on the degree of similarity, each node can assign 1-4 notes. Each note was treated as a unique node (for example, four radiologists could label the object as a node, resulting in four notes), and 4,252 nodes were selected from the LIDC data set. The radiologist recorded 158 lung nodes in the UCLA data set and used them in this study. Each knee is a positive sample for the classification of pulmonary buds. Draw negative (nodular) examples from the method. Use multi-level thresholds and morphological operations to find a large number of candidates[29]. Perform rule-based analysis to remove extremely small or large candidates beyond the target detection range (5 mm to 30 mm). Candidate institutions for tuberculosis and non-tuberculosis for classification follow the conventions from previous papers.

LATC-IDRI and UCLA datasets, including scanning, are provided with a variety of diagnostic methods. For better pixel measurements, all CT scans were first converted to a Hounsfield Unit (HU) scale using information on the DICOM module and then converted to a (0.1) level of (-1000, 500 HU). Removed 3D cube measuring 40 × 40 × 40 mm or individually for recording. Each cube is focused on those who will be registered. 40 mm was selected so that all entrants could enter the category because the largest fields in our group were about 30 mm. Then, each cube with a pixel size that did not change in all three dimensions is removed, resulting in isotropic cubes at all times[30]. The central parts of this cube in the axial, sagittal, and coronal view are now collected as 2.5D of the internet.

4 Results and Evaluation

During the workshop, both the CNN model hybrid ensemble and the HSCNN model were developed exercising the Xavier set of rules and simplified by the Adam stochastic optimization set of rules. To record the maximum power of the node while reducing the input dimension, the input candidate size of the cube is set to 52x52x52. The CNN model uses a 2.5D input with a size of 52x52x3. The HSCNN model uses the entire 3D cube as input. In both cases, the learning rate was 0.001. Choose the most common plan. The hyper-scale was selected with a detailed grid search and validation data set for the first 20 days. Both models are implemented in the Python 2.7 as well as the Tensor Flow and Keras manuals. All research was conducted on a server with 16 Intel Xeon E5-2630 CPUs, 32GB of memory, and an NVIDIA TITAN Xp GPU (12GB of storage).

4.1 Analysis

One of the limitations of CNN's hybrid approach is that the model relies on the production process for obtaining separate election masks such as production data. Therefore, the pre-selection step selects the upper sensor limit for the next node analysis (configuration)[31]. If the nodes are deficient in the electoral generation stage, the planned type will not find them. Under current conditions, the generation of nucleation candidates is an independent component to fix it. Future work will explore the interconnected, end-of-the-lung pipeline that combines the steps of nuclear election production and nuclear acquisition in the traditional form of in-depth study. In this general case, these two steps can be improved and improved by reducing training errors in one form.

There are limits to HSCNN training. Basically, the properties of lobulation and speculation nodule are well-known properties associated with lung cancer, but they cannot be used in this study due to typographical errors found in LIDC. Second, the primary semantic components have a scale of 5 or 6; name change, the change in binary type may be lost in some label information[32]. Using binary labels instead of keywords is still important for this purpose. However, the main point solves the problem of labels, wherever the amount of instances infected with a definite scale can be actual trivial associated to another scale (for example, only four cases are listed as popcorn statistics, when 3018 cases were registered missing in the statistical standard.). Second, the analysis shows that the reader's agreement is very low on a scale of 5 or 6 compared to that produced by the binary. Thus, writing names helps to reduce writing noise caused by differences in readers[33]. One way to overcome these two shortcomings is to gather a big dot with semantic names. Although only five modules have been developed for the HSCNN framework in this article, the HSCNN design and the total loss process can be easily extended to increase or decrease the number of low-level semantic components. Future work will explore the development of the model, add additional semantic written resources and explore geographical differences using a different writing schedule. More information about future jobs will be provided.

Finally, the ability to analyze CARS images is demonstrated in human lung tissue using in-depth CNN pre-trained ImageNet records. Transport training is used to prevent recurrence of the pattern and make a different classification between ordinary and lung cancer tissues over and above diverse lung cancers. The typical processing time for envisaging an image is no less than half a second[34]. By providing an effective discrepancy identification of lung cancer, permitting clinicians to acquire basic knowledge in concurrent, and step up the clinical assessment, the reported unlabeled computerized imaging strategies have the potential to have a significant clinical effect. In combination with fiber-based imaging probes, this approach will diminish the prerequisite for tissue biopsy and help with ultimate cure. This approach is mainly limited by statistics and can be supplementary amended by having a larger and added general amount of data to verify the technology within the entire distribution of lung lesions and spectrum found in clinical practice.

5 Results and Discussion

This paper reports the prerequisite for tools and techniques to help physicians work on screening to optimize lung cancer diagnosis, improve the accuracy of cancer diagnosis, and reduce radiation costs and exposure[35]. Our approach is to develop techniques for automated lung segmentation, nodule classification, cancer diagnosis, and estimation of individual regular screening intervals[36]. The specific contributors to this treatise are:

Improves the accuracy of detection of pleural nodules with a method of pulmonary segmentation without parameters. A new approach to lung segmentation is being introduced, using a bidirectional chain code coupled to a machine learning system. Neural network of a reliable hybrid set for classification of pulmonary nodules. A hybrid functional neural network is developed in this study that differentiates between pulmonary nodules and, improving model reliability using VGG module sets, residual modules, and closely related module designs. It can be interpreted as a hierarchical semantically convergent neural network for the diagnosis of lung cancer. It is described in this study how field knowledge could be incorporated into the planned in-depth learning framework so that the model can be interpreted and improved in the diagnosis of lung cancer. Statistical models are used to estimate different disease states. It is shown how the new Bayesian structure can be used to obtain more accurate and reliable estimates of disease progression by observing errors.

Into the bargain, this approach is common to all activities, including inverted / convex detection. For example, in MRI, a regional/convex analysis can identify and differentiate the epithelium from the epithelium to identify the risk of concussion[37]. Regardless of whether the additional information has been posted or the external information has been posted, the amount of information collected and the various constructive changes indicate significant impact. This model can be used to train muscles, but it can also be a strength. HSCNN predicts the onset of gastrointestinal symptoms and the first gastrointestinal function to be examined[38]. The HSCNN module was able to compare these encoded encodings in a red-and-read format for incorrect integration. Predictable semantic signals were important in explaining expressions that indicate abnormal behaviors and correlate with medical knowledge known to treat lung and lung cancer. The built-in mode can be used as a built-in generator for illegal troubles. This paper stipulates a method to increase the classification of MST for specific cohorts and visual cues under false observation[39]. In the experimental clinics, with the collected research data (potentially noisy and amplified), this work enabled a precise description of the trial time. It also serves as a basis for the progress of individual screening, as screening work will be offered for every field. In this classification process, advanced machines and an in-depth learning model are trained and evaluated by reducing the number of training, certification, and testing. Training was used to reduce training errors and to improve test standards. Validation was used to match the hyper model. The final evaluation of the model's performance for the exams is reported as external results. The design ensures that independent tests are not taught by training the model with good explanations and that the performance of the model must be clearly shown without disclosure[40]. Remember that basic search in only uses training and validation during cross-validation, regardless of performance tests; It can be said that such designs have output data and thus tend to compare performance.

Although much effort has been ensured to improve the described methods, additional research can be used to improve these methods. As already discussed, advanced lung dissection sometimes prevents the inclusion of pleural nodules located at the site of compaction. One approach to elucidate this setback is to administer a postoperative solution based on the area after receiving the first mask to separate the lungs. Markov fields of conditional randomness are one of the methods that can be used for this purpose. At the same time, advances in in-depth learning techniques may further explore controversial area-based and pixel-based neural networks for lung dissection to treat juxtaposed neural nodules. Another limitation of the separation method is that the standard inclusion point detection and peripheral correction distortion were performed separately on each 2D image board. One possible extension of this function is the detection of 3D inclusion points and 3D correction of the two lobes. 3D information can be used to further reduce cross-separation / under-separation errors.

A deep learning model for the diagnosis and classification of pulmonary nodules has been developed and is effective. Nonetheless, traditional pulmonary isolation, isolation of prospective pulmonary nodules, classification of pulmonary nodules, and diagnosis of pulmonary nodules developed independently (i.e., as independent components). Recent advances in multifunctional learning and semantic separation provide the opportunity to complete pulmonary separation, nodule detection, cancer diagnosis, and nodular circulation in one framework. For example, He et al. developed the R-CNN mascara method for detection, segmentation, and separation of semantic objects in one deep learning model. The R-CNN mask can form the basis for the development of a multifunctional model for pulmonary anatomy, node detection, cancer diagnosis, and nodular circulation.

In addition, the current model of lung examination only has two signs: nodular and nodular. The extension of these functions allows the identification of multiple categories using additional tags (e.g., delivery). This multi-stage setup contains additional determinants that could potentially improve the function of the models in lung examination. This semantic production function allows human experts now easily read and comment on the feasibility of this semantic production. There are ways to present models using active learning techniques that involve human strategies to improve the accuracy of models for cancer diagnosis. There will be more scripts and files in the future, and more scripts or labels can be used to provide other information. In this case, product label information can be included in the design to make it robust. Therefore, it is necessary to develop a research model that meets the mathematical requirements of semantic tasks in future work. Note that not all semantic character combinations can be combined to convey the experience in the name. Therefore, it can be analyzed to improve design parameters. Finally, the introduction to the standard model is a 3B measurement of the average value of each sample and the intensity of each subsequent pixel. Subsequent outcomes, such as pulmonary edema of the cervical, thoracic nodes, may prevent the model from examining important career data. Future effort is to deal with the practice of an in-depth learning model with node protection in a node (background) environment as two independent combinations of each data entry.

Conflicts of Interest

The Author(s) declare(s) that there is no conflict of interest throughout in this study.

References

1. Kim, J. S., Kim, J. H., Cho, G., & Bae, K. T. (2005). Automated detection of pulmonary nodules on CT images: effect of section thickness and reconstruction interval—initial results. Radiology, 236(1), 295-299..
2. Kim, S., Erwin, D., & Wu, D. (2012). Efficacy of dual lung cancer screening by chest x-ray and sputum cytology using Johns Hopkins Lung Project Data. Journal of Biometrics and Biostatistics, 3(03)..
3. Kaya, A., & Can, A. B. (2015). A weighted rule based method for predicting malignancy of pulmonary nodules by nodule characteristics. Journal of biomedical informatics, 56, 69-79..
4. Krupinski, E. A., Berbaum, K. S., Caldwell, R., & Schartz, K. M. (2012, February). Is diagnostic accuracy for detecting pulmonary nodules in chest CT reduced after a long day of reading?. In Medical Imaging 2012: Image Perception, Observer Performance, and Technology Assessment (Vol. 8318, p. 83180X). International Society for Optics and Photonics..
5. Kingma, D. P., & Ba, J. (2014). Adam: A method for stochastic optimization. arXiv preprint arXiv:1412.6980..
6. Ko, J. P., & Betke, M. (2001). Chest CT: automated nodule detection and assessment of change over time—preliminary experience. Radiology, 218(1), 267-273..
7. Jiang, H., Walter, S. D., Brown, P. E., & Chiarelli, A. M. (2016). Estimation of screening sensitivity and sojourn time from an organized screening program. Cancer epidemiology, 44, 178-185..
8. Jackson, C. H., Sharples, L. D., Thompson, S. G., Duffy, S. W., & Couto, E. (2003). Multistate Markov models for disease progression with classification error. Journal of the Royal Statistical Society: Series D (The Statistician), 52(2), 193-209..
9. Jorritsma, W., Cnossen, F., & van Ooijen, P. M. (2015). Improving the radiologist–CAD interaction: designing for appropriate trust. Clinical radiology, 70(2), 115-122..
10. Jia, J., Barbera, L., & Sutradhar, R. (2016). Using Markov multistate models to examine the progression of symptom severity among an ambulatory population of cancer patients: are certain symptoms better managed than others?. Journal of pain and symptom management, 51(2), 232-239.
11. Jing, Z., Bin, L., & Lianfang, T. (2010, September). Lung nodule classification combining rule-based and SVM. In 2010 IEEE fifth international conference on bio-inspired computing: theories and applications (BIC-TA) (pp. 1033-1036). IEEE..
12. Jackson, C. (2011). Multi-state models for panel data: the msm package for R. Journal of statistical software, 38, 1-28..
13. Andersen, P. K., Hansen, L. S., & Keiding, N. (1991). Assessing the influence of reversible disease indicators on survival. Statistics in Medicine, 10(7), 1061-1067..
14. Hinton, G. E., & Salakhutdinov, R. R. (2006). Reducing the dimensionality of data with neural networks. science, 313(5786), 504-507.,.
15. Ali, A. M., El-Baz, A. S., & Farag, A. A. (2007, April). A novel framework for accurate lung segmentation using graph cuts. In 2007 4th IEEE International Symposium on Biomedical Imaging: From Nano to Macro (pp. 908-911). IEEE..
16. Abadi, M., Barham, P., Chen, J., Chen, Z., Davis, A., & Dean, J. (2016). Ma◎ hieu Devin, Sanjay Ghemawat, Geoffrey Irving, Michael Isard, et al.". Tensorflow: a system for large-scale machine learning." In: OSDI, 16, 265-283..
17. Ge, Z., Sahiner, B., Chan, H. P., Hadjiiski, L. M., Cascade, P. N., Bogot, N., ... & Zhou, C. (2005). Computer-aided detection of lung nodules: false positive reduction using a 3D gradient field method and 3D ellipsoid fitting. Medical physics, 32(8), 2443-2454.

18. Gilbert, F. J., Astley, S. M., Gillan, M. G., Agbaje, O. F., Wallis, M. G., James, J., ... & Duffy, S. W. (2008). Single reading with computer-aided detection for screening mammography. New England Journal of Medicine, 359(16), 1675-1684..
19. Armato III, S. G., Altman, M. B., Wilkie, J., Sone, S., Li, F., Doi, K., & Roy, A. S. (2003). Automated lung nodule classification following automated nodule detection on CT: A serial approach. Medical Physics, 30(6), 1188-1197..
20. Funahashi, K. I., & Nakamura, Y. (1993). Approximation of dynamical systems by continuous time recurrent neural networks. Neural networks, 6(6), 801-806..
21. Froz, B. R., de Carvalho Filho, A. O., Silva, A. C., de Paiva, A. C., Nunes, R. A., & Gattass, M. (2017). Lung nodule classification using artificial crawlers, directional texture and support vector machine. Expert Systems with Applications, 69, 176-188..
22. Esteva, A., Kuprel, B., Novoa, R. A., Ko, J., Swetter, S. M., Blau, H. M., & Thrun, S. (2017). Dermatologist-level classification of skin cancer with deep neural networks. nature, 542(7639), 115-118..
23. Erasmus, J. J., Connolly, J. E., McAdams, H. P., & Roggli, V. L. (2000). Solitary pulmonary nodules: Part I. Morphologic evaluation for differentiation of benign and malignant lesions. Radiographics, 20(1), 43-58..
24. Day, N. E., & Walter, S. D. (1984). Simplified models of screening for chronic disease: estimation procedures from mass screening programmes. Biometrics, 1-13..
25. Dilger, S. K., Uthoff, J., Judisch, A., Hammond, E., Mott, S. L., Smith, B. J., ... & Sieren, J. C. (2015). Improved pulmonary nodule classification utilizing quantitative lung parenchyma features. Journal of Medical Imaging, 2(4), 041004..
26. Duffy, S. W. (2005). Screening, sojourn time. Encyclopedia of Biostatistics, 7..
27. Deng, L., Seltzer, M. L., Yu, D., Acero, A., Mohamed, A. R., & Hinton, G. (2010). Binary coding of speech spectrograms using a deep auto-encoder. In Eleventh Annual Conference of the International Speech Communication Association..
28. Doi, K. (2005). Current status and future potential of computer-aided diagnosis in medical imaging. The British journal of radiology, 78(suppl_1), s3-s19..
29. Das, M., Mühlenbruch, G., Mahnken, A. H., Flohr, T. G., Gündel, L., Stanzel, S., ... & Wildberger, J. E. (2006). Small pulmonary nodules: effect of two computer-aided detection systems on radiologist performance. Radiology, 241(2), 564-571..
30. Dahl, G., Ranzato, M. A., Mohamed, A. R., & Hinton, G. E. (2010). Phone recognition with the mean-covariance restricted Boltzmann machine. Advances in neural information processing systems, 23..
31. Dhara, A. K., Mukhopadhyay, S., Alam, N., & Khandelwal, N. (2013, February). Measurement of spiculation index in 3D for solitary pulmonary nodules in volumetric lung CT images. In Medical Imaging 2013: Computer-Aided Diagnosis (Vol. 8670, p. 86700K). International Society for Optics and Photonics..
32. Duffy, S. W., Chen, H. H., Tabar, L., & Day, N. E. (1995). Estimation of mean sojourn time in breast cancer screening using a Markov chain model of both entry to and exit from the preclinical detectable phase. Statistics in medicine, 14(14), 1531-1543..
33. Bae, K. T., Kim, J. S., Na, Y. H., Kim, K. G., & Kim, J. H. (2005). Pulmonary nodules: automated detection on CT images with morphologic matching algorithm—preliminary results. Radiology, 236(1), 286-293..
34. Bengio, Y. (2009). Learning deep architectures for AI. Now Publishers Inc..
35. Bengio, Y., Courville, A., & Vincent, P. (2013). Representation learning: A review and new perspectives. IEEE transactions on pattern analysis and machine intelligence, 35(8), 1798-1828..
36. Bergstra, J., & Bengio, Y. (2012). Random search for hyper-parameter optimization. Journal of machine learning research, 13(2)..
37. Bottou, L., & Bousquet, O. (2007). The tradeoffs of large scale learning. Advances in neural information processing systems, 20..
38. Annangi, P., Thiruvenkadam, S., Raja, A., Xu, H., Sun, X., & Mao, L. (2010, April). A region based active contour method for x-ray lung segmentation using prior shape and low level features. In 2010 IEEE international symposium on biomedical imaging: from nano to macro (pp. 892-895). IEEE..
39. Armato III, S. G., & Sensakovic, W. F. (2004). Automated lung segmentation for thoracic CT: impact on computer-aided diagnosis1. Academic Radiology, 11(9), 1011-1021..
40. Armato III, S. G., Roberts, R. Y., Kocherginsky, M., Aberle, D. R., Kazerooni, E. A., MacMahon, H., ... & Clarke, L. P. (2009). Assessment of radiologist performance in the detection of lung nodules: dependence on the definition of "truth". Academic radiology, 16(1), 28-38.